Recent advances in liquid phase transmission electron microscopy of nanoparticle growth and self-assembly

Joodeok Kim,[†] Sungsu Kang,[†] Fanrui Cheng,[†] Yi Wang, Xingchen Ye,* and Jungwon Park*

Over the last several decades, colloidal nanoparticles have evolved into a prominent class of building blocks for materials design. Important advances include the synthesis of uniform nanoparticles with tailored compositions and properties, and the precision construction of intricate, higher-level structures from nanoparticles via self-assembly. Grasping the modern complexity of nanoparticles and their superstructures requires fundamental understandings of the processes of nanoparticle growth and self-assembly. *In situ* liquid phase transmission electron microscopy (TEM) has significantly advanced our understanding of these dynamic processes by allowing direct observation of how individual atoms and nanoparticles interact in real time, in their native phases. In this article, we highlight diverse nucleation and growth pathways of nanoparticles in solution that could be elucidated by the *in situ* liquid phase TEM. Furthermore, we showcase *in situ* liquid phase TEM studies of nanoparticle self-assembly pathways, highlighting the complex interplay among nanoparticles, ligands, and solvents. The mechanistic insights gained from *in situ* liquid phase TEM investigation could inform the design and synthesis of novel nanomaterials for various applications such as catalysis, energy conversion, and optoelectronic devices.

Introduction

Colloidal nanoparticles and superstructures of nanoparticles have been increasingly used in diverse applications such as catalysis,[1,2] optoelectronics,[3,4] and biomedical applications,[5,6] owing to their unique physical and chemical properties. These applications are enabled by significant advances in (1) the synthesis of colloidal nanoparticles with tailored size, shape, and compositions;[7–11] and (2) the construction of superstructures from individual nanoparticles via self-assembly.[12–14] On the other hand, the synthesis of novel nanoparticles with near-atomic precision, chemical compositions, and improved uniformity necessitates mechanistic understanding of the nanoparticle growth process. Furthermore, the design and construction of self-assembled nanoparticle superstructures require understanding of the complex interactions among nanoparticles, surface ligands, solvent, and the substrate.[15] Therefore, mechanistic insights of the kinetic pathways of nanoparticle formation and assembly are crucial for the design and predictive synthesis of novel nanomaterials.

In situ transmission electron microscopy (TEM) has provided important clues to the structural dynamics of nanoparticles, including growth, self-assembly, diffusion, dissolution, and shape transformations under vacuum, liquid, and gas environments,[14,16–21] by allowing for the observation of temporal series dynamics of individual nanoparticles in real space and real time. In particular, liquid phase (LP) TEM enables the direct, real-time observations

Joodeok Kim, School of Chemical and Biological Engineering and Institute of Chemical Processes, Seoul National University, Seoul, Republic of Korea; Center for Nanoparticle Research, Institute for Basic Science (IBS), Seoul, Republic of Korea; juori22@snu.ac.kr

Sungsu Kang, School of Chemical and Biological Engineering and Institute of Chemical Processes, Seoul National University, Seoul, Republic of Korea; Center for Nanoparticle Research, Institute for Basic Science (IBS), Seoul, Republic of Korea; sungsukang@snu.ac.kr

Fanrui Cheng, Department of Chemistry, Indiana University Bloomington, Bloomington, USA; chengf@iu.edu

Yi Wang, Department of Chemistry, Indiana University Bloomington, Bloomington, USA; yw90@iu.edu

Xingchen Ye, Department of Chemistry, Indiana University Bloomington, Bloomington, USA; xingye@indiana.edu

Jungwon Park, School of Chemical and Biological Engineering and Institute of Chemical Processes, Seoul National University, Seoul, Republic of Korea; Center for Nanoparticle Research, Institute for Basic Science (IBS), Seoul, Republic of Korea; Institute of Engineering Research, College of Engineering, Seoul National University, Seoul, Republic of Korea; Advanced Institute of Convergence Technology, Seoul National University, Suwon, Gyeonggi, Republic of Korea; jungwonpark@snu.ac.kr

*Corresponding author

[†] Joodeok Kim, Sungsu Kang, and Fanrui Cheng have equally contributed to this work.

of nanoparticles in solutions by encapsulating the samples in a thin liquid layer within a liquid cell. A key component of the liquid cells is a pair of thin electron-transparent windows, typically made of amorphous silicon nitride (SiN_x) or graphene. They have high electron transparency and mechanical strength enabling electrons to pass through and generate high-resolution images while preventing the sample solution from evaporating. Dry-state TEM after quenching the nanoparticle solution under reactions can alter the structure and properties of intermediate species.[22,23] It is also difficult to investigate the structure of individual nanoparticles using spectroscopy or diffractometry, which provide structural information averaged over nanoparticle ensemble.[24–27] Recent advances in *in situ* LPTEM have enabled deeper understanding on the formation and self-assembly processes of nanoparticles in liquid, revealing nonclassical growth pathways of nanoparticles,[28] which were not predicted by classical nucleation theory (CNT). Complex self-assembly processes of nanoparticles in liquid governed by long-range, nonadditive interactions[29,30] have also been investigated extensively by *in situ* LPTEM.[31–36]

In this article, we discuss experimental findings of growth and self-assembly of nanoparticles by *in situ* LPTEM, and explain the results in terms of nonclassical nucleation and growth pathways. First, we summarize experimental evidence of nonclassical pathways in nanoparticle growth and describe diverse growth pathways of nanoparticles revealed by *in situ* LPTEM observations. Second, we highlight some important observations of nanoparticle self-assembly processes and explain the underlying interactions between nanoparticles during crystallization. Finally, we discuss future challenges and opportunities in understanding nanoparticle growth and self-assembly via *in situ* LPTEM. Although we focus on recent *in situ* LPTEM observations of nucleation, growth, and self-assembly of nanoparticles in solutions, we also highlight several *in situ* high-resolution TEM studies conducted under a high vacuum. The high vacuum condition minimizes electron scattering from the samples and enables atomic-scale TEM observations of nanoparticles, providing valuable insights into the nanoparticle nucleation and growth.

In situ TEM investigation of nanoparticle growth

The process of nanoparticle formation can be divided into a nucleation stage, where monomers (single ions or their complexes) condense to form nuclei, and a growth stage, where the nuclei grow into larger crystals (**Figure** 1a).[37–39] CNT explains an important mechanistic pathway observed in the growth of colloidal nanoparticles,[40–42] by assuming spherical nuclei and equilibrium conditions. CNT suggests that the overall growth rate is regulated by size-dependent surface energy after overcoming the critical free energy barrier through nucleation (Figure 1b, green curve). A narrow size distribution is typically achieved at high monomer concentrations during growth because the growth rate is inversely proportional to the nanoparticle sizes, whereas "Ostwald ripening" becomes dominant as monomers deplete.[43] Although CNT has shown good qualitative agreement with experimental results,[44,45] it

has limitations when the surface structure and morphology of nanoparticles becomes important because CNT based on the Gibbs–Thomson model does not take into account structural attributes at the single-particle level. Nanoparticles often have nonspherical shapes, and the system deviates from equilibrium conditions especially during the early stages of nucleation. Relatively stable nanoclusters or prenucleation clusters identified during the synthesis of various nanoparticles cannot be explained by CNT, which describes only one energy barrier.[25,46–49] Rather, those observations suggest the presence of a nonclassical nucleation pathway with multiple local minima in the energy landscape (Figure 1b, blue curve).[47–49] By understanding the nanoparticle formation mechanism, researchers have demonstrated that the synthesis of nanoparticles with desired structures is possible with high uniformity.[50,51] However, the identification and characterization of those intermediates are difficult unless they are particularly stable, allowing them to be isolated during the synthesis. Thus, it is necessary to directly observe the nucleation and growth stages of nanoparticle formation *in situ*.

Nucleation stage
A relatively common structural feature observed by *in situ* LPTEM is the intermediates of lower-symmetry or amorphous structures that crystallize into the larger nanoparticles with a bulk crystal structure.[52–56] In a study using LPTEM, Loh et al. observed a multistep nonclassical nucleation and growth pathway for Au nanoparticles.[52] First, a dense liquid phase containing more Au precursors forms from the homogeneous liquid phase, and then amorphous Au nanoparticles are formed from the dense liquid phase. These amorphous Au intermediates then coalesce to form crystalline Au nanoparticles. High-resolution TEM unambiguously identified the dense liquid phase, amorphous solid, and crystalline solid, providing important insights into the multistep nucleation pathways. Similarly, Yang et al. also observed amorphous-phase-mediated crystallization of Ni nanoparticles.[57] The authors used graphene liquid cells (GLCs), which enable LPTEM imaging at higher resolution by encapsulating a nanoparticle solution between two graphene sheets.[58] During the crystallization of Ni nanoparticles on graphene, amorphous Ni nanoparticles initially form from a homogeneous precursor solution and subsequently, crystalline domains nucleate from the Ni nanoparticle surface and propagate to the entire nanoparticle (Figure 1c). Theoretical calculations showed that relatively low surface energy of amorphous Ni and its interaction with graphene stabilize the amorphous state of Ni. Also, multiple nucleation of the crystalline domains within a single Ni nanoparticle results in the formation of polycrystalline nanoparticle (Figure 1d), implying the possible role of the nonclassical nucleation in the formation of polycrystalline nanoparticles. The nucleation behavior of metallic nanoparticles can be influenced by the elements consisting the nanoparticle and chemical environment such as the presence and type of ligands and reducing agents. Sun et al. observed the growth mechanism
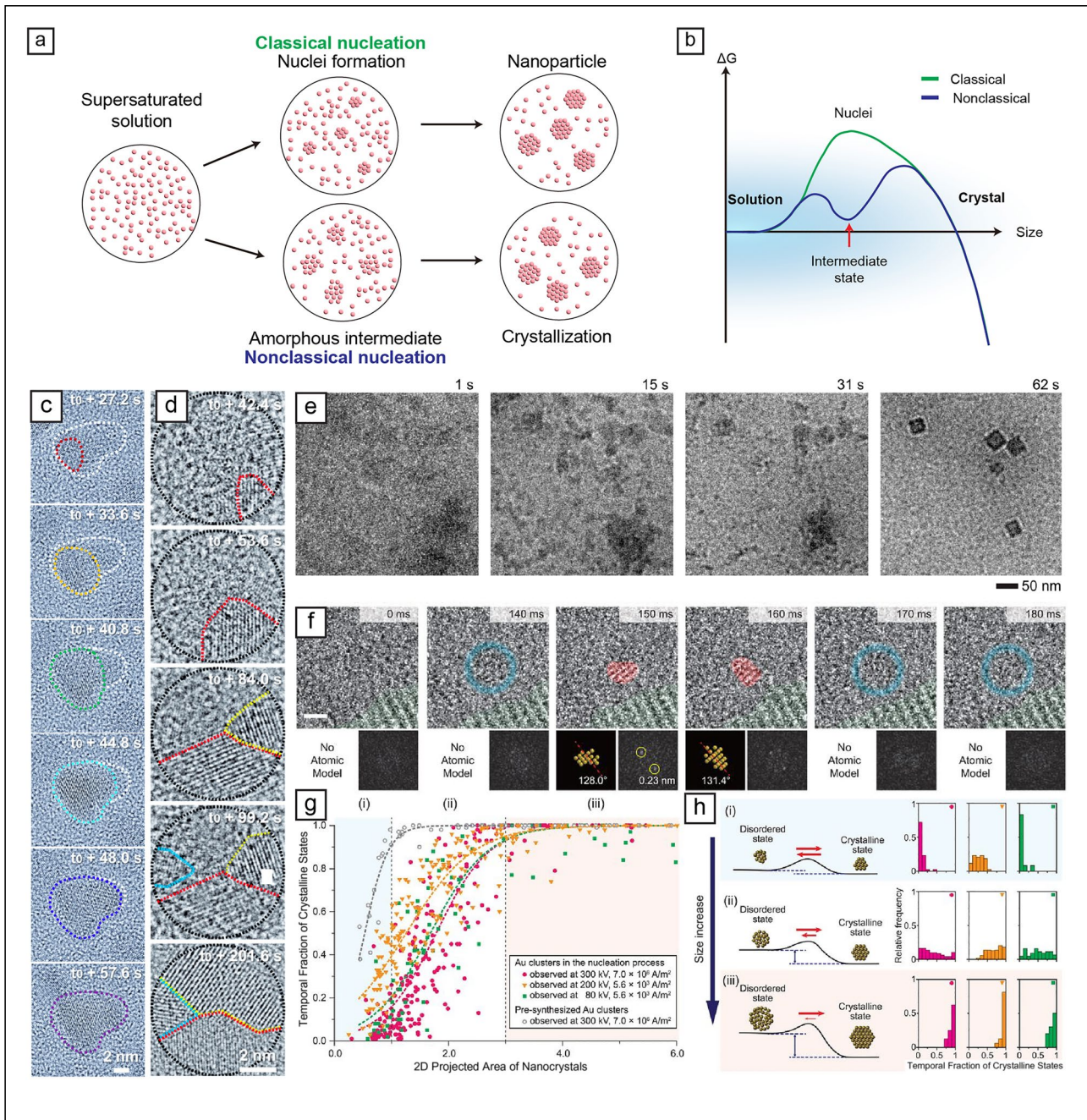
Figure 1. *In situ* liquid phase transmission electron microscopy (TEM) studies of investigating nonclassical nucleation. (a) The schematics of the mechanism of particle nucleation in the classical nucleation versus nonclassical nucleation, amorphous to crystalline. (b) Energy landscapes for classical nucleation theory and nonclassical nucleation theory. (c, d) A time series of TEM images shows the growth of the crystalline area from the amorphous intermediate of Ni nanoparticle. (e) Time series images of ZIF-8 nanocube nucleation and crystallization processes. (f) Sequential images of the gold nanoparticle nucleation process observed under a high vacuum condition with FFT images and corresponding atomic model. Blue circles indicate a disordered (amorphous) state, and red colors indicate the crystalline areas of the gold nanoparticle. Scale bar = 1 nm. (g) The proportion of time during which crystallinity is observed in the 2D projection of a Au nanoparticle's nucleation process and particles synthesized *ex situ* (illustrated by gray circles) is measured. The dashed lines on the graph are logistic models fitting the data. (h) Characteristics of nanoclusters varying with size throughout the nucleation phase. (Left) Illustrative energy diagrams present the transition of nucleation behavior across nanocrystals ranging from small (i) to large (iii). (Right) Distribution charts of the crystalline state occurrences over time for three distinct cluster sizes and under varying imaging scenarios, as referenced in (h). (c–h) Reprinted with permission from Reference 57. © 2019 American Chemical Society. Reprinted with permission from Reference 63. © 2021 National Academy of Sciences. Reprinted with permission from Reference 87. © 2021 AAAS.

of high-entropy alloy nanoparticles in the presence of sodium borohydride and thiol ligands in solution.[59] They suggested that the aggregation of subnanometer clusters is a dominant mechanism in the growth of high-entropy alloy nanoparticles with a strong reducing agent.

Nonclassical nucleation pathways in nonmetallic nanoparticles have also been demonstrated.[36,60–63] Yang et al. reported the multistep formation mechanism of 2D transition-metal oxide nanosheets in the presence of oleylamine ligands.[64] The transition-metal oxide 2D nanosheets emerge via two steps: first, molecular precursors dissolved in the solution undergo nucleation and growth to form 3D nanoparticles; then, closely spaced 3D nanoparticles undergo the 3D-to-2D transformation, followed by the aggregation into a larger transition-metal oxide nanosheet. The 3D-to-2D transformation occurs due to the size-dependent competition between negative (100) surface energy and positive (110) surface energy when these surfaces are passivated with ligands. This work confirms the importance of surface energy modulation by passivating ligands and demonstrates the role of thermodynamics in nanoparticle growth through free energy minimization. Nielsen et al. pioneered the use of *in situ* LPTEM and observed the multiple growth pathways of $CaCO_3$, which are relevant in biomineralization.[60] In their work, they showed the $CaCO_3$ formation by both the direct and indirect pathways mediated by amorphous and crystalline intermediates, involving the formation of an amorphous precursor followed by a consequent crystallization process.

In LPTEM, the electron beam induces radiolysis of liquid, changing the solvent chemistry,[65–67] which can significantly affect the chemical bonds with high ionic properties. It is thus essential to use a low electron dose to study the nucleation of nanoparticles of ionic compounds. Liu et al. reported a three-step nucleation mechanism for metal–organic frameworks (MOFs), mediated by dense liquid phase and amorphous clusters (Figure 1e).[63] Due to the electron-beam sensitivity of MOF,[68,69] the authors used a low electron dose rate of 0.05 e$^-$ Å^{-2} s^{-1} and kept the cumulative dose to be lower than 5 e$^-$ Å^{-2}. Furthermore, the continuous injection of the fresh solution using a syringe pump likely reduced the concentration of radiolytic products. The crystallization of MOF nanoparticles starts from the phase separation of dense liquid phase containing precursors from the homogeneous precursor solution, after which the dense liquid phases condense into amorphous clusters. Finally, the amorphous cluster crystallizes into 100-nm-sized MOF nanoparticles. The authors could not perform detailed structural characterization of the intermediate states due to the beam sensitivity. Instead, they aimed to support the presence of the dense liquid phase and amorphous clusters, and the absence of crystallinity using cryo-TEM and electron diffraction.

The nucleation of nanoparticles in liquid occurs by the reduction of metal ions, or the binding of ionic monomers. However, these processes are strongly influenced by the chemistry of the liquid where the electron beam is irradiated and radiolytic products are formed.[70–74] For example, gold nanoparticles can form or dissolve in liquid depending on the dose rate and the pH of the initial solvent.[75] Numerical simulation models based on chemical equilibrium and reaction kinetics have been used to estimate the radiolysis products and their concentrations,[66,76] but chemical equilibrium in liquid cells under the high-energy radiation may differ significantly from ambient conditions.[77] The type of liquid cell also impacts the chemistry within. At the surface of SiN_x membranes, there are silanol (SiOH) and silylamine (Si_2NH and $SINH_2$) functional groups that are protonated and deprotonated at different pH levels and electron dose rates,[78–80] critically influencing the nanoparticle movement on the SiN_x membranes through electrostatic interactions.[78,81,82] Research suggested that in GLCs, the graphene surface is functionalized differently from the SiN_x surface under electron-beam irradiation, reducing the electrostatic interaction with the liquid cell substrate and nanoparticles.[83] In addition to those efforts, further research would be needed to understand the actual chemistry during LPTEM imaging. From the experimental perspective, the use of ultralow dose rate conditions is advantageous by minimizing the unwanted electron-beam effects. Employing spatial filters[63,68] or advanced image processing algorithms[84,85] can be beneficial for reducing the noise of *in situ* TEM data taken under such low dose rate conditions.

The diffusion coefficient is one of the key parameters in crystallization theories. Studies calculating the diffusion coefficients of nanoparticles, including those in SiN_x liquid cells and GLCs, showed that the diffusion process in a liquid cell differs from that in bulk solution, and is influenced by the electron-beam dose rate.[78,81–83] These differences in diffusion rate are expected to affect the local supersaturation ratio of precursors, the concentration of radical species, and the interaction between nanoparticles, thus influencing the nucleation and growth processes of the nanoparticles. Introducing a flow within a liquid cell by injecting solution can facilitate the diffusion within the liquid cell and may quench unwanted radiolytic products. On the other hand, the relatively slow flow rate and the presence of dead volume where the flow is not reached within the liquid cell suggest that the design of the current liquid cells needs to be further advanced.

During nucleation, individual atoms are added to the as-formed nuclei continuously. Achieving atomic resolution in LPTEM is challenging due to the liquid's thickness and that of the cell windows unless they are sufficiently thin.[86] Recently, a detailed mechanistic understanding of nonclassical nucleation pathway has been demonstrated by Jeon et al. at temporal resolution down to 1.6 ms while retaining atomic resolution.[87] They prepared AuCN nanoribbons that decompose into Au monomers (possibly single ions or atoms) when irradiated by an electron beam on graphene in a high vacuum condition. The monomers form Au nanoparticles spontaneously, and the aberration-corrected TEM images captured at high frame rates exhibit the reversible transformation of small Au nanoparticles

(around 1 nm) between crystalline and disordered states during the growth of the Au nanoparticles (Figure 1f). Because a slight rotation of crystalline Au nanoparticle can make the crystal planes of gold nanoparticles deviate from the viewing direction, atomic modeling and TEM simulation were performed to show that the nanoparticles have a disordered structure when they do not show even slight lattice patterns in the projected TEM images. The temporal fraction of the disordered states decreases as the nanoparticles grow by the addition of atoms, and Au nanoparticles larger than 2 nm mostly remain in a crystalline state (Figure 1g). This result shows that disordered nanoparticles are metastable, and the energy difference between the crystalline states and metastable disordered states becomes larger with an increasing nanoparticle size (Figure 1h).

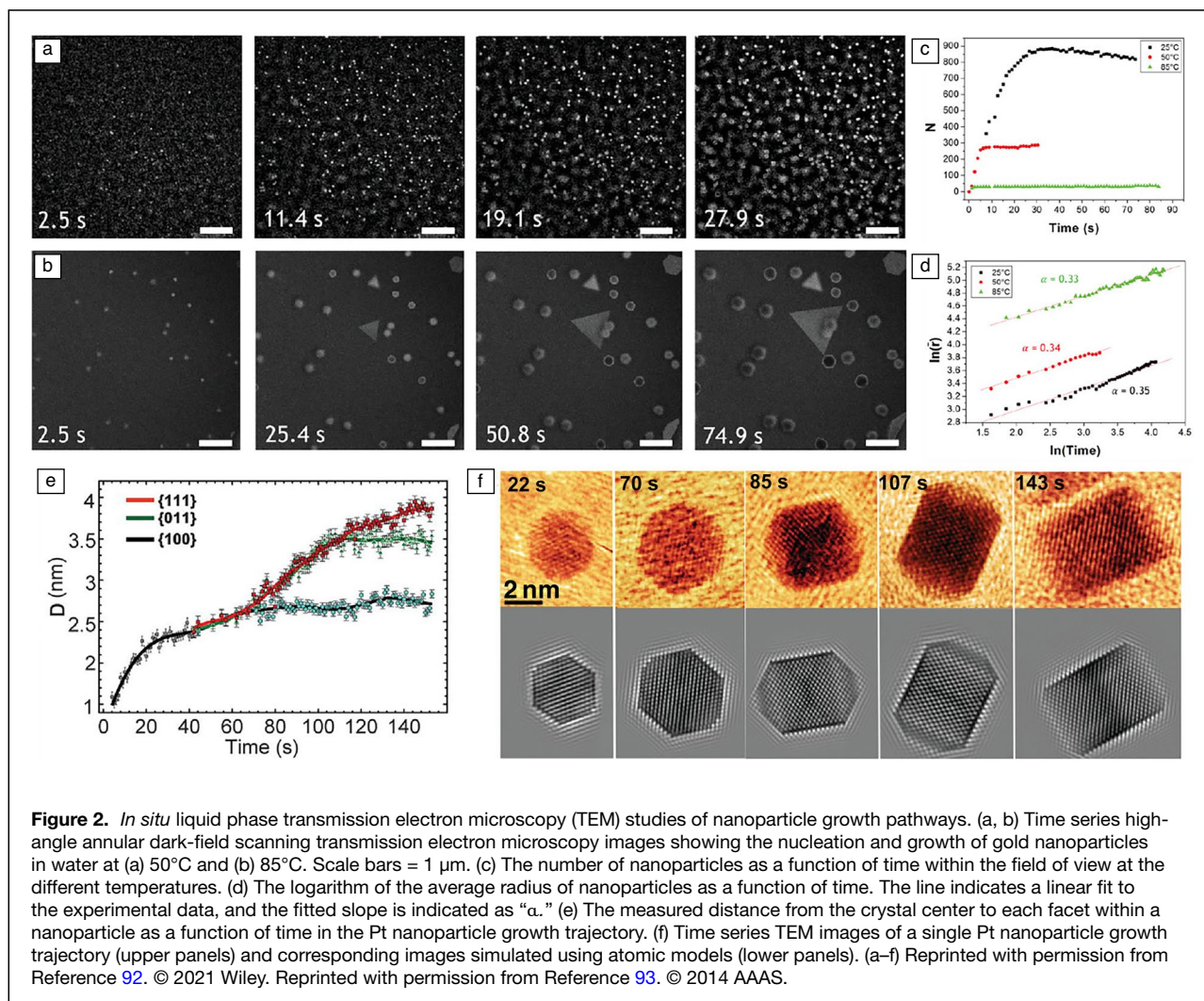### Growth pathways of nanoparticles

After the formation of nuclei, the nuclei grow into nanoparticles through both the classical, monomeric attachment pathway as well as nonclassical pathways. To fully understand the nanoparticle growth pathway with *in situ* LPTEM, tracking single particles is essential. Additionally, trajectory analysis of a statistical number of nanoparticles is required.[28,36,70,88–90]

Woehl et al. quantitatively analyzed the growth of 300–500 silver nanoparticles in liquid and explained the growth mechanism using the Lifshitz–Slyozov–Wagner (LSW) model,[91] which describes a classical Ostwald ripening process. However, the LSW model did not fit well with the shape of the experimental particle size distribution (PSD) due to the coalescence between nanoparticles, a nonclassical growth pathway that has been observed by *in situ* LPTEM. Instead, the authors adopted Smoluchowski aggregation kinetics, which describes the successive, diffusion-limited aggregation reactions of particles, and successfully and quantitatively explained PSD. More recently, Khelfa et al. quantitatively analyzed the growth mechanism of gold nanoparticles using liquid phase scanning TEM (STEM) with heating equipment to investigate thermal effects on the nanoparticle growth.[92] The gold nanoparticles were synthesized at different temperatures (25°C, 50°C, and 85°C) in liquid cells using the electron beam and exhibited size variations corresponding to these temperatures (**Figure 2**a–b). In this case, gold nanoparticles were adhered to the SiN$_x$ membranes and did not show coalescence between them. Thus, the authors explained nanoparticle growth trajectories with the LSW model (Figure 2c–d). At 50°C and 85°C when the nanoparticles are motionless, the nanoparticle growth is governed by diffusion-limited growth, and the activation energy for nanoparticle growth is successfully predicted. Also, they observed Ostwald ripening and revealed that thermo-activated Ostwald ripening process does not solely depend on size effect.

At a single-particle scale, crystalline nanoparticles are often faceted by exposing crystal surfaces with low surface energies, unlike the assumptions of CNT. Thus, the growth of nanoparticles is expected to occur to reduce the overall surface energy by first removing high-surface-energy surfaces. The growth anisotropy of nanoparticles was first demonstrated by Liao et al. who observed Pt nanoparticle growth in liquid at lattice-resolving resolution using SiN$_x$ liquid cells.[93] The authors confirmed that the growth rate of each facet can be predicted from surface energy minimization theories. Due to the interaction between ethylamine ligands and surfaces, {011}, {110}, and {111} facets of Pt nanoparticles exhibit similar surface energy when they are smaller than 5 nm, showing spherical growth (Figure 2e–f). However, when the size exceeds a critical threshold, ethylamine ligands block the {100} facets, hindering growth in that direction. This results in the formation of cubic nanoparticles. Gao et al. observed similar dynamics in the nucleation and growth of Pt over Pd nanocubes terminated with {100} facets using LPTEM.[94] The Pd {100} facets are covered by Br$^-$ ions, and the growth predominantly occurred at the corners of the Pd nanocubes. When the Pt reaches a threshold thickness (1.6 nm), surface diffusion of Pt at the corners happens to cover {100} surfaces.
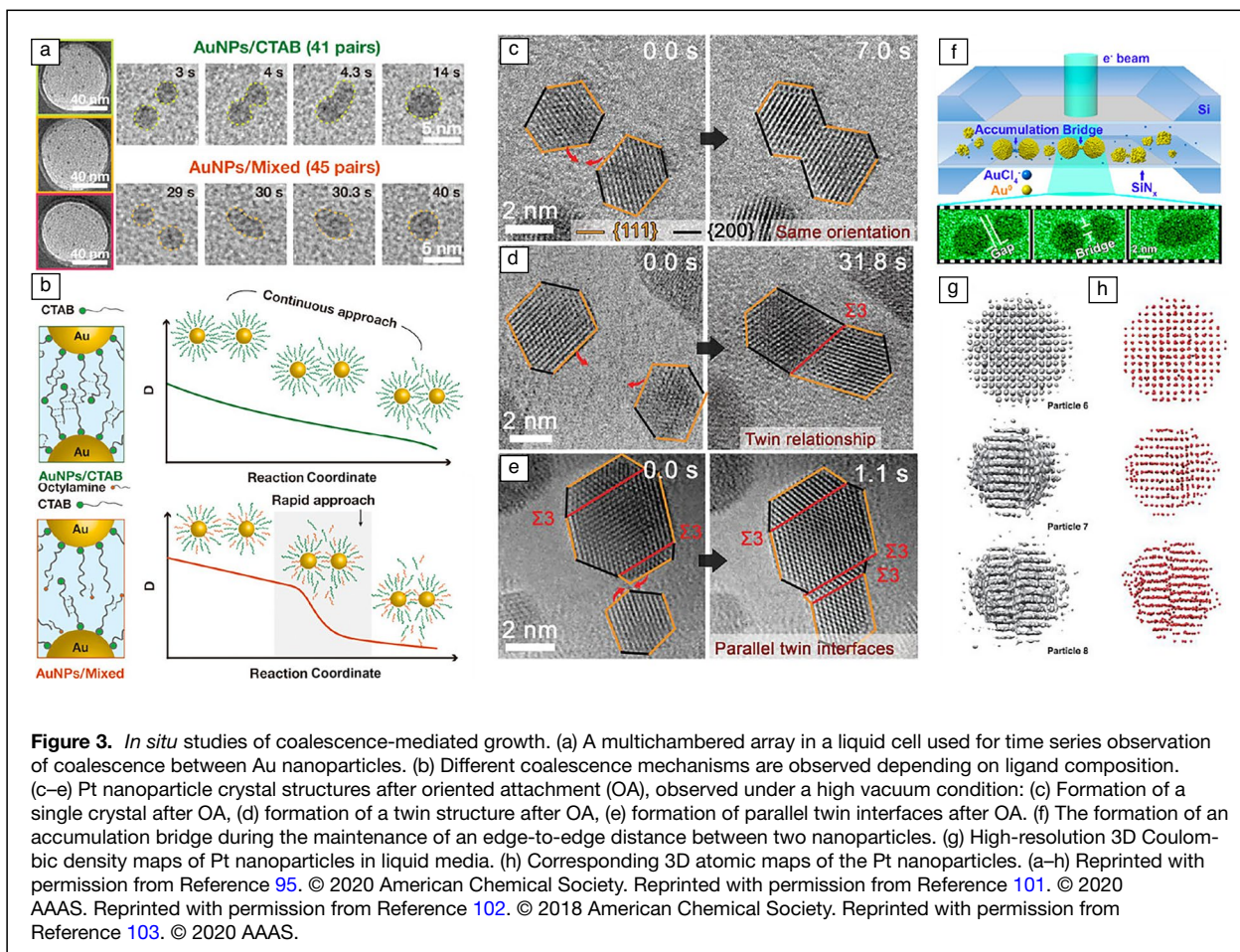
Single-particle visualization by *in situ* LPTEM has also revealed coalescence-mediated growth of nanoparticles and the structural changes in the nanoparticles involved in the coalescence. Zheng et al. first visualized the coalescence-mediated growth of Pt nanoparticles in SiN$_x$ liquid cells, highlighting the important role of coalescence in nanoparticle growth.[88] They demonstrated that monomeric growth and coalescence mediated growth concurrently occur in liquid media. After the coalescence process, the growth rate of the nanoparticle becomes slower, and both pathways lead to a nearly monodisperse distribution in terms of size. Yuk et al. using LPTEM with GLCs, observed the coalescence events between nanoparticles, which results in the formation of nanoscale twin boundaries in single Pt nanoparticles.[58] Although GLCs are an efficient tool to investigate the nonclassical growth pathways of nanoparticles in liquids with higher resolution, it is often challenging to observe multiple nanoparticles using GLCs for statistical analysis of growth trajectories due to the random formation of liquid pockets. Lim et al. developed multichambered GLCs based on a large-scale array of ordered chambers using anodic aluminum oxide (AAO). This design provides physical separation between each chamber, allowing for multiple efficient experiments within a single liquid cell to quantitatively analyze coalescence between nanoparticles (**Figure 3**a).[95] Using this multichamber liquid cell, Bae et al. investigated the coalescence behaviors of gold nanoparticles passivated with different ligands (CTAB and CTAB/octylamine) in liquid.[96] Analysis of each nanoparticle-ligand system reveals differences in coalescence dynamics between the two ligand systems. When the two nanoparticles coalesce, they form a dumbbell-like shape by creating a neck at the interface, and the dumbbell-shaped nanoparticles undergo relaxation to be a spherical shape. The authors revealed that the nanoparticles passivated only with CTAB undergo faster relaxation due to the difference in ligand mobility in each ligand system (Figure 3b).

Figure 2. *In situ* liquid phase transmission electron microscopy (TEM) studies of nanoparticle growth pathways. (a, b) Time series high-angle annular dark-field scanning transmission electron microscopy images showing the nucleation and growth of gold nanoparticles in water at (a) 50°C and (b) 85°C. Scale bars = 1 μm. (c) The number of nanoparticles as a function of time within the field of view at the different temperatures. (d) The logarithm of the average radius of nanoparticles as a function of time. The line indicates a linear fit to the experimental data, and the fitted slope is indicated as "α." (e) The measured distance from the crystal center to each facet within a nanoparticle as a function of time in the Pt nanoparticle growth trajectory. (f) Time series TEM images of a single Pt nanoparticle growth trajectory (upper panels) and corresponding images simulated using atomic models (lower panels). (a–f) Reprinted with permission from Reference 92. © 2021 Wiley. Reprinted with permission from Reference 93. © 2014 AAAS.

For crystalline nanoparticles, the crystal planes of the nanoparticles can affect the coalescence behavior.[97,98] Coalescence by oriented attachment (OA), in which the alignment of crystal planes of two nanoparticles occurs prior to the attachment, is also a main topic in nonclassical nanoparticle growth observed in LPTEM,[36,99] as proposed by Penn and Banfield.[100] Li et al. observed multiple coalescence events of ferrihydrite nanoparticles.[36] They demonstrated that the coalescence happens after the rotation of the nanoparticles in liquid until the lattice planes match to each other. When the lattice planes of two ferrihydrite nanoparticles are misaligned, the energy barrier will be high, preventing the attachment of the two particles, while the alignment of crystal planes of two nanoparticles makes the energy barrier low. The OA process leads to the formation of single-crystalline nanoparticles, but it is possible for nanoparticles with a low twin-boundary energy to coalesce at imperfect lattice alignment, leaving twin boundaries after the coalescence. Song et al. investigated a twinning mechanism from OA of Au nanoparticles embedded in a mobile solid matrix with *in situ* high-resolution TEM in a high vacuum condition,

explaining the origin of fivefold twins.[101] They proposed two fivefold twinning mechanisms: decomposition of high-energy grain boundaries and slipping of partial dislocations. In both cases, nanoparticles form a twin boundary after the OA process, and further OA of the twinned nanoparticle can result in a fivefold twin (Figure 3c–e). Jin et al. introduced a novel mechanism of coalescence in the presence of an Au precursor in liquid.[102] In a comparison of the "jump-to-contact" mechanism in the OA process, they demonstrated that between two adjacent nanoparticles, the edge-to-edge distance between them remains unchanged, but a nanobridge forms spontaneously between the nanoparticles and accelerates fusion of the nanoparticles (Figure 3f).

The grain boundaries in nanoparticles are likely to form by the coalescence of two nanoparticles with imperfect lattice alignment. Park et al. using "Brownian one-particle reconstruction" method, visualized twist grain boundaries between {110} and {100} planes in three dimensions.[103] Kim et al. advanced the same methodology to atomic resolution, enabling investigation of atomic structures of distorted

Figure 3. *In situ* studies of coalescence-mediated growth. (a) A multichambered array in a liquid cell used for time series observation of coalescence between Au nanoparticles. (b) Different coalescence mechanisms are observed depending on ligand composition. (c–e) Pt nanoparticle crystal structures after oriented attachment (OA), observed under a high vacuum condition: (c) Formation of a single crystal after OA, (d) formation of a twin structure after OA, (e) formation of parallel twin interfaces after OA. (f) The formation of an accumulation bridge during the maintenance of an edge-to-edge distance between two nanoparticles. (g) High-resolution 3D Coulombic density maps of Pt nanoparticles in liquid media. (h) Corresponding 3D atomic maps of the Pt nanoparticles. (a–h) Reprinted with permission from Reference 95. © 2020 American Chemical Society. Reprinted with permission from Reference 101. © 2020 AAAS. Reprinted with permission from Reference 102. © 2018 American Chemical Society. Reprinted with permission from Reference 103. © 2020 AAAS.

lattices and grain boundaries in single Pt nanoparticles (Figure 3g–h).[104] These results suggest that nanoparticle formation involves various 2D defects and lattice disorder, in addition to relatively stable twin boundaries. Thus, we believe that further research on the nanoparticle growth process, which results in grain boundaries and lattice disorders will be necessary in the future.

LPTEM studies have expanded our knowledge of nanoparticle nucleation and growth and provided deep insights into nanoparticle synthesis by directly observing phenomena that were previously unrecognized. For example, LPTEM has unambiguously shown the presence of multistep, nonclassical growth pathways in nanoparticle synthesis. Recent bulk nanoparticle synthesis studies have demonstrated that the structure of the resulting nanoparticles can be precisely controlled by controlling the structure of intermediates in the multistep nanoparticle growth.[50,51] On the other hand, further application of the LPTEM to bulk nanoparticle synthesis, through the development of a quantitative nanoparticle growth theory, requires the statistical observations of the nanoparticle growth trajectories possibly aided by machine learning-based image analysis.[85,105] This will have an increasing impact on bulk wet chemistry

studies of nanoparticle synthesis. Furthermore, statistical LPTEM observations of nanoparticles, combined with the development of a quantitative nanoparticle growth theory, will allow us to compare the differences between LPTEM environments and bulk nanoparticle synthesis environments, further accounting for possible differences between the liquid cell and bulk conditions in wet synthesis.

In situ TEM investigation of nanoparticle self-assembly

Bottom-up assembly of nanoscale objects such as nanocrystals, macromolecules, and proteins into macroscopic structures is a central theme in chemistry, materials science, and biology. Self-assembly can produce sophisticated nano- and mesostructures with a precision that rivals existing lithographic methods. Studies of kinetic pathways and mechanisms of self-assembly have largely relied on the electron microscopy analysis of the final static structures or indirect monitoring using scattering techniques such as small-angle x-ray scattering.[106,107] While real-time video microscopy has been a common method in studying the assembly of micron-sized colloids,[108] analogous tools for probing the self-assembly dynamics of colloidal nanoparticles have been lacking until the recent invention of the

LPTEM technique. In the past decade, several research groups have utilized LPTEM to study self-assembly of nanoparticles that were either premade or formed *in situ*.[109–118] In 2012, Alivisatos and co-workers reported *in situ* LPTEM imaging of 2D nanoparticle superlattice formation (**Figure 4**a).[119] The nanoparticles were slowly diffusing and their assembly was driven mainly by capillary forces and solvent fluctuations, which was consistent with lattice-gas simulation results. Later, the same group observed ionic-strength-tuned, tip-to-tip assembly of charge-stabilized gold nanorods mediated by long-range electrostatic repulsion (Figure 4b).[32] By tracking and analyzing the trajectories of many individual nanorods, they were able to extract the mathematical form of the interaction potential between nanorods (Figure 4c). In 2017, Chen and co-workers applied low-dose-rate LPTEM to image the assembly process of gold triangular nanoprisms.[120] Through quantitative analyses of superstructure size distributions, they found that the self-assembly kinetics followed the growth laws of reaction-limited step-growth polymerization (Figure 4d). Later, the same group demonstrated *in situ* LPTEM observation of large-scale superlattice formation from charged gold nanoprisms (Figure 4e).[34] The assembly process was triggered by electron-beam irradiation, which increased the local ionic strength due to radiolysis and more effectively screened the electrostatic repulsions among nanoprisms. By combining

particle tracking analyses with computer simulations, they uncovered that the translational ordering of the superlattices emerged from orientational randomness among the nanoprisms of individual columns. Furthermore, they found that the assembly proceeded through a nonclassical crystallization pathway involving an amorphous, dense intermediate phase. As another example, Li and co-workers studied the self-assembly dynamics of silver nanoparticles in aqueous solutions (Figure 4f).[30] By combining liquid cell TEM imaging with AFM-based force measurements and theoretical calculations, they showed that the superlattice formation was governed by the interplay between the short-ranged steric hindrance and hydration forces and long-ranged electric double-layer repulsive and van der Waals forces.

Besides self-assembly in the aqueous phase, *in situ* LPTEM has also been utilized to study nanoparticle assembly in nonaqueous solutions. For example, Zheng and co-workers captured the assembly process of FePt nanoparticles into a low-density, 2D hexagonal lattice (**Figure 5**a).[113] From particle tracking and diffusion analyses, they were able to quantify the magnitude of forces between the particles and showed that long-range anisotropic forces likely drive the formation of nanoparticle chains. More recently, Ye and co-workers reported polymer-grafted nanoparticles suspended in various organic solvents as model systems for studying
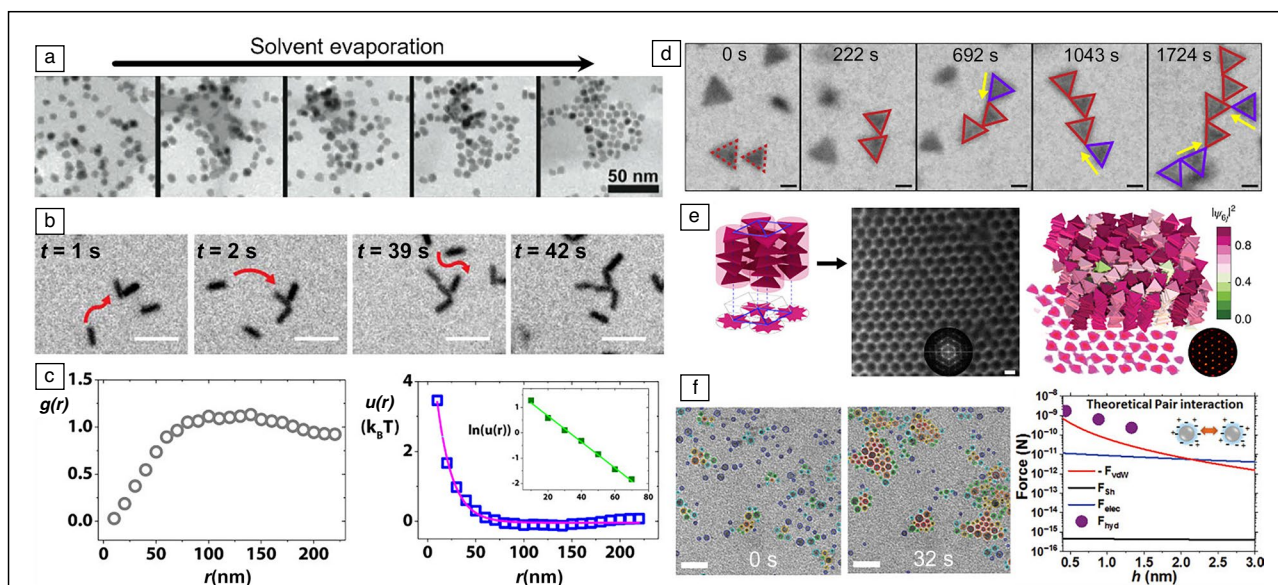
Figure 4. *In situ* liquid phase transmission electron microscopy (TEM) studies of nanoparticle interactions and self-assembly. (a) *In situ* TEM snapshots of 2D superlattice formation from Pt nanoparticles. (b) Time-lapse TEM images showing tip-to-tip attachment of gold nanorods. Scale bars = 100 nm. (c) Pair distribution function *g*(*r*) versus *r* plot (left) and pairwise interaction energy *u*(*r*) versus *r* plot with its exponential fitting (right). Scale bars = 50 nm. (d) Time-lapse TEM images showing chain growth of gold triangular nanoprisms. Scale bars = 50 nm. (e) Schematic illustration of self-assembling nanoprisms into a hexagonal lattice consisting of stacked nanoprisms columns (left), *in situ* TEM image showing the highly ordered hexagonal lattice (middle), and computer simulations of the hexagonal lattice formation (right). Scale bar = 100 nm. (f) Time-lapse TEM images of self-assembling Ag nanoparticles (left) and calculated interparticle forces as a function of particle separation *h* (right). Scale bars = 10 nm. (a–f) Reprinted with permission from Reference 119. © 2012 American Chemical Society. Reprinted with permission from Reference 32. © 2015 American Chemical Society. Reprinted with permission from Reference 120. © 2017 Springer Nature. Reprinted with permission from Reference 34. © 2020 Springer Nature. Reprinted with permission from Reference 30. © 2019 Wiley.
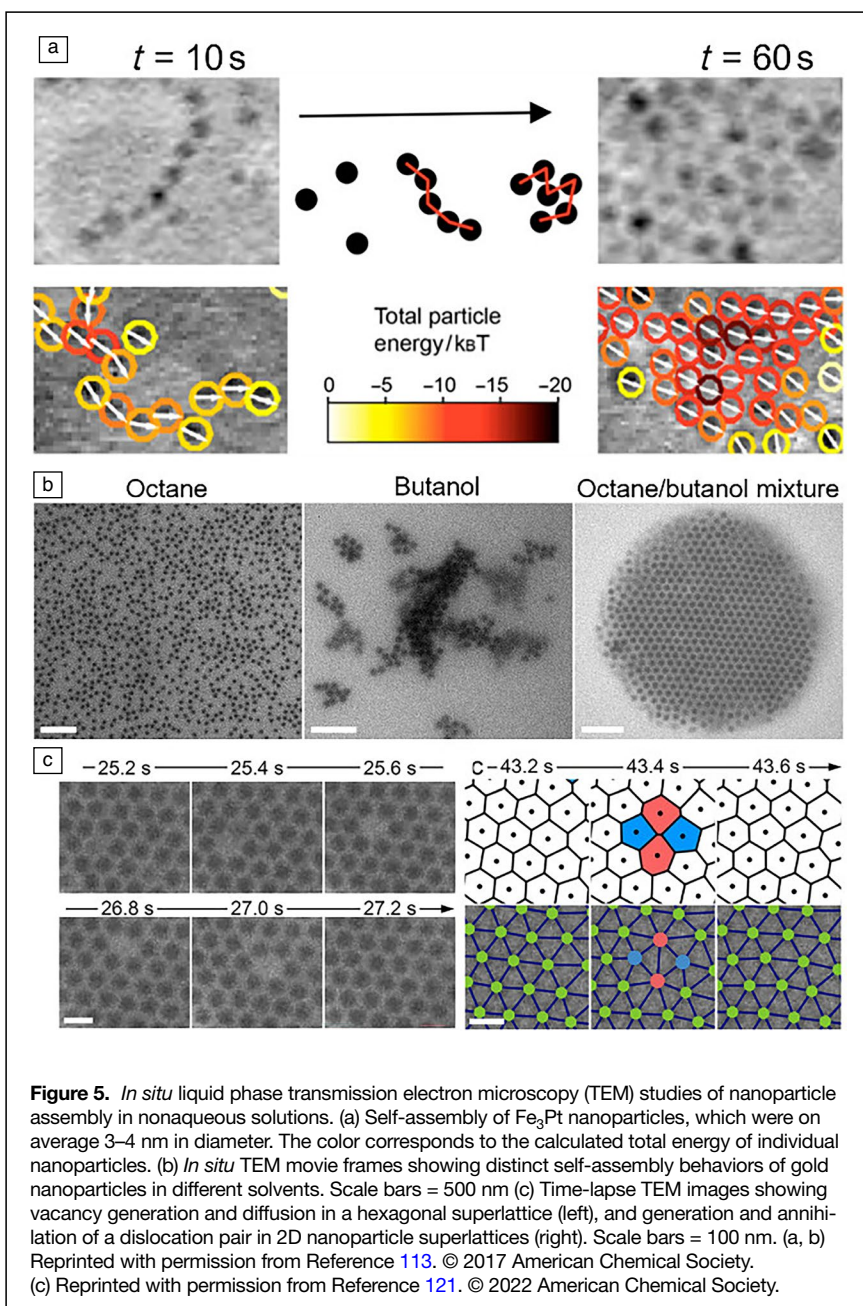
nanoparticle self-assembly into highly ordered superlattices with LPTEM.[121] They demonstrated that electron-beam irradiation activates nanoparticle motion and controls nanoparticle diffusivity, while the nature of the solvent largely dictates nanoparticle interactions and their self-assembly pathways (Figure 5b). Multiorder-parameter analysis revealed a multistep crystallization pathway consisting of four distinct stages, namely, gas state, cluster state, polycrystalline, and single-crystalline solid states. They further analyzed the formation, migration, and annihilation of distinct types of structural defects in 2D nanoparticle superlattices (Figure 5c). They elucidated that long-range interactions, including van der Waals attraction and electrostatic repulsion dictate the observed assembly behavior whereas interactions between polymer brushes were insignificant. These findings pave the way toward independent control of LPTEM imaging conditions and nanoparticle self-assembly conditions.

Despite considerable progress, several challenges in LPTEM study of nanoparticle self-assembly remain to be addressed. First, the ever-present electron-beam–sample interactions should be carefully accounted for to ensure accurate interpretation of results and minimize potential artifacts.[118] Although direct probing of molecular-level radiation chemistry specifics during LTEPM is not always feasible, well-designed systematic studies (e.g., dependence on electron dose rate or solution pH) can often be conducted to shed light on the mechanism and robustness of any intriguing phenomena observed under a particular LPTEM condition. Second, the interaction between nanoparticles and the liquid cell window surface should be precisely controlled (e.g., via electron dose rate or solution conditions) to prevent nanoparticles from strongly adhering to the window thus reducing their mobility, and at the same time, to prevent nanoparticles being expelled from the imaging area due to electrostatic repulsion. Third, to leverage the benefits of changing the chemical environment within the liquid flow cell, the hydrodynamic properties of the LPTEM flow system should be thoroughly characterized through experiments and numerical modeling.[108] Fourth, it remains extremely difficult to replicate conventional drying-mediated (or evaporation-driven) self-assembly of nanoparticles with LPTEM. However, the insights gained from LPTEM experiments on the "nanoparticle interaction potential–self-assembly kinetic pathway–final superstructure" relationships are relevant and can often be translatable to self-assembly studies outside TEM. We believe that LPTEM holds the potential to further revolutionize our understanding of novel nanoscale self-assembly dynamics. Examples include directed self-assembly (e.g., light-driven, electric field-driven, etc.), nonequilibrium active soft matter, and more.

Figure 5. *In situ* liquid phase transmission electron microscopy (TEM) studies of nanoparticle assembly in nonaqueous solutions. (a) Self-assembly of Fe_3Pt nanoparticles, which were on average 3–4 nm in diameter. The color corresponds to the calculated total energy of individual nanoparticles. (b) *In situ* TEM movie frames showing distinct self-assembly behaviors of gold nanoparticles in different solvents. Scale bars = 500 nm (c) Time-lapse TEM images showing vacancy generation and diffusion in a hexagonal superlattice (left), and generation and annihilation of a dislocation pair in 2D nanoparticle superlattices (right). Scale bars = 100 nm. (a, b) Reprinted with permission from Reference 113. © 2017 American Chemical Society. (c) Reprinted with permission from Reference 121. © 2022 American Chemical Society.

Conclusion and outlook

In summary, we provide a critical review of the fascinating and rapidly evolving fields of nanoparticle growth and self-assembly studied by LPTEM. Compared to top-down lithography

approaches, colloidal synthesis and self-assembly promises scalability and precise control of building blocks down to the atomic and single-particle levels. As a real-space and real-time imaging technique with high spatiotemporal resolution, LPTEM is uniquely positioned to elucidate the kinetic pathways of nanoparticle nucleation, growth and superstructure formation via self-assembly, which can offer critical insights to the realization of materials-by-design. Propelled by the rapid advances in electron detectors, machine learning, especially deep learning techniques,[85,121] as well as design and fabrication of new liquid cell architectures, we anticipate transformative changes in the field of LPTEM in the coming decade.

Acknowledgments

Author contributions

All authors have contributed to the preparation of the manuscript.

Funding

Competing interests

The authors declare that they have no competing interests.

Open Access

References

1. D. Astruc, *Chem. Rev.* **120**, 461 (2020)
2. C. Xie, Z. Niu, D. Kim, M. Li, P. Yang, *Chem. Rev.* **120**, 1184 (2020)
3. Y. Shirasaki, G.J. Supran, M.G. Bawendi, V. Bulović, *Nat. Photonics* **7**, 13 (2013)
4. F.P. García de Arquer, D.V. Talapin, V.I. Klimov, Y. Arakawa, M. Bayer, E.H. Sargent, *Science* **373**, eaaz8541 (2021)
5. D.A. Giljohann, C.A. Mirkin, *Nature* **462**, 461 (2009)
6. N. Lee, D. Yoo, D. Ling, M.H. Cho, T. Hyeon, J. Cheon, *Chem. Rev.* **115**, 10637 (2015)
7. A.R. Tao, S. Habas, P. Yang, *Small* **4**, 310 (2008)
8. Y. Xia, X. Xia, H.-C. Peng, *J. Am. Chem. Soc.* **137**, 7947 (2015)
9. Y. Shi, Z. Lyu, M. Zhao, R. Chen, Q.N. Nguyen, Y. Xia, *Chem. Rev.* **121**, 649 (2021)
10. A.L. Efros, L.E. Brus, *ACS Nano* **15**, 6192 (2021)
11. R.G. Chaudhuri, S. Paria, *Chem. Rev.* **112**, 2373 (2012)
12. J.J. De Yoreo, P.U.P.A. Gilbert, N.A.J.M. Sommerdijk, R.L. Penn, S. Whitelam, D. Joester, H. Zhang, J.D. Rimer, A. Navrotsky, J.F. Banfield, A.F. Wallace, F.M. Michel, F.C. Meldrum, H. Cölfen, P.M. Dove, *Science* **349**, aaa6760 (2015)
13. X. Ye, J. Chen, M.E. Irrgang, M. Engel, A. Dong, S.C. Glotzer, C.B. Murray, *Nat. Mater.* **16**, 214 (2017)
14. M.A. Boles, M. Engel, D.V. Talapin, *Chem. Rev.* **116**, 11220 (2016)
15. D. Li, Q. Chen, J. Chun, K. Fichthorn, J. De Yoreo, H. Zheng, *Chem. Rev.* **123**, 3127 (2023)
16. Q. Chen, J.M. Yuk, M.R. Hauwiller, J. Park, K.S. Dae, J.S. Kim, A.P. Alivisatos, *MRS Bull.* **45**(9), 713 (2020)
17. P.A. Crozier, T.W. Hansen, *MRS Bull.* **40**(1), 38 (2015)
18. B. Luo, J.W. Smith, Z. Ou, Q. Chen, *Acc. Chem. Res.* **50**, 1125 (2017)
19. S. Rackauskas, S.D. Shandakov, H. Jiang, J.B. Wagner, A.G. Nasibulin, *Sci. Rep.* **7**, 12310 (2017)
20. S.B. Simonsen, I. Chorkendorff, S. Dahl, M. Skoglundh, J. Sehested, S. Helveg, *J. Am. Chem. Soc.* **132**, 7968 (2010)
21. L. Chen, A. Leonardi, J. Chen, M. Cao, N. Li, D. Su, Q. Zhang, M. Engel, X. Ye, *Nat. Commun.* **11**, 3041 (2020)
22. Y. Du, H. Sheng, D. Astruc, M. Zhu, *Chem. Rev.* **120**, 526 (2020)
23. M.S. Bootharaju, W. Baek, S. Lee, H. Chang, J. Kim, T. Hyeon, *Small* **17**, 2002067 (2021)
24. J. Polte, T.T. Ahner, F. Delissen, S. Sokolov, F. Emmerling, A.F. Thünemann, R. Kraehnert, *J. Am. Chem. Soc.* **132**, 1296 (2010)
25. B.H. Kim, K. Shin, S.G. Kwon, Y. Jang, H.S. Lee, H. Lee, S.W. Jun, J. Lee, S.Y. Han, Y.H. Yim, D.H. Kim, T. Hyeon, *J. Am. Chem. Soc.* **135**, 2407 (2013)
26. B. Abécassis, C. Bouet, C. Garnero, D. Constantin, N. Lequeux, S. Ithurria, B. Dubertret, B.R. Pauw, D. Pontoni, *Nano Lett.* **15**, 2620 (2015)
27. N.G. Bastús, J. Comenge, V. Puntes, *Langmuir* **27**, 11098 (2011)
28. H.G. Liao, L. Cui, S. Whitelam, H. Zheng, *Science* **336**, 1011 (2012)
29. C.A.S. Batista, R.G. Larson, N.A. Kotov, *Science* **350**, 1242477 (2015)
30. J. Lee, E. Nakouzi, D. Xiao, Z. Wu, M. Song, C. Ophus, J. Chun, D. Li, *Small* **15**, 1901966 (2019)
31. Z. Wang, C. Liu, Q. Chen, *J. Cryst. Growth* **601**, 126955 (2023)
32. Q. Chen, H. Cho, K. Manthiram, M. Yoshida, X. Ye, A.P. Alivisatos, *ACS Cent. Sci.* **1**, 33 (2015)
33. J. Kim, M.R. Jones, Z. Ou, Q. Chen, *ACS Nano* **10**, 9801 (2016)
34. Z. Ou, Z. Wang, B. Luo, E. Luijten, Q. Chen, *Nat. Mater.* **19**, 450 (2020)
35. L. Liu, E. Nakouzi, M.L. Sushko, G.K. Schenter, C.J. Mundy, J. Chun, J.J. De Yoreo, *Nat. Commun.* **11**, 1045 (2020)
36. D. Li, M.H. Nielsen, J.R.I. Lee, C. Frandsen, J.F. Banfield, J.J. De Yoreo, *Science* **336**, 1014 (2012)
37. K.J. Klabunde (ed.), *Nanoscale Materials in Chemistry* (Wiley, Hoboken, 2001)
38. G. Schmid (ed.), *Nanoparticles: From Theory to Application* (Wiley, Weinheim, 2010)
39. S.G. Kwon, T. Hyeon, *Small* **7**, 2685 (2011)
40. P.G. Debenedetti, *Metastable Liquids: Concepts and Principles* (Princeton University Press, Princeton, 1996)
41. D.W. Oxtoby, *J. Phys. Condens. Matter* **4**, 7627 (1992)
42. N.T.K. Thanh, N. Maclean, S. Mahiddine, *Chem. Rev.* **114**, 7610 (2014)
43. J.A. Marqusee, J. Ross, *J. Chem. Phys.* **79**, 373 (1983)
44. C.B. Murray, D.J. Norris, M.G. Bawendi, *J. Am. Chem. Soc.* **115**, 8706 (1993)
45. T. Sugimoto, *Adv. Colloid Interface Sci.* **28**, 65 (1987)
46. P. Dagtepe, V. Chikan, J. Jasinski, V.J. Leppert, *J. Phys. Chem. C* **111**, 14977 (2007)
47. H.S. Chen, R.V. Kumar, *J. Phys. Chem. C* **113**, 31 (2009)
48. D. Gebauer, A. Völkel, H. Cölfen, *Science* **322**, 1819 (2008)
49. D.C. Gary, M.W. Terban, S.J.L. Billinge, B.M. Cossairt, *Chem. Mater.* **27**, 1432 (2015)
50. L. Qiao, N. Pollard, R.D. Senanayake, Z. Yang, M. Kim, A.S. Ali, M.T. Hoang, N. Yao, Y. Han, R. Hernandez, A.Z. Clayborne, M.R. Jones, *Nat. Commun.* **14**, 4408 (2023)
51. Y. Kim, H. Choi, Y. Lee, W. Koh, E. Cho, T. Kim, H. Kim, Y.-H. Kim, H.Y. Jeong, S. Jeong, *Nat. Commun.* **12**, 4454 (2021)

52. N.D. Loh, S. Sen, M. Bosman, S.F. Tan, J. Zhong, C.A. Nijhuis, P. Král, P. Matsudaira, U. Mirsaidov, *Nat. Chem.* **9**, 77 (2017)
53. H.E.M. Hussein, R.J. Maurer, H. Amari, J.J.P. Peters, L. Meng, R. Beanland, M.E. Newton, J.V. Macpherson, *ACS Nano* **12**, 7388 (2018)
54. B. Jin, Y. Wang, Z. Liu, A. France-Lanord, J.C. Grossman, C. Jin, R. Tang, *Adv. Mater.* **31**, 1808225 (2019)
55. W. Dachraoui, T.R. Henninen, D. Keller, R. Erni, *Sci. Rep.* **11**, 23965 (2021)
56. W. Dachraoui, M.I. Bodnarchuk, R. Erni, *ACS Nano* **16**, 14198 (2022)
57. J. Yang, J. Koo, S. Kim, S. Jeon, B.K. Choi, S. Kwon, J. Kim, B.H. Kim, W.C. Lee, W.B. Lee, H. Lee, T. Hyeon, P. Ercius, J. Park, *J. Am. Chem. Soc.* **141**, 763 (2019)
58. J.M. Yuk, J. Park, P. Ercius, K. Kim, D.J. Hellebusch, M.F. Crommie, J.Y. Lee, A. Zettl, A.P. Alivisatos, *Science* **336**, 61 (2012)
59. J. Sun, A. Leff, Y. Li, T.J. Woehl, *Nanoscale* **15**, 10447 (2023)
60. M.H. Nielsen, S. Aloni, J.J. De Yoreo, *Science* **345**, 1158 (2014)
61. P.J.M. Smeets, K.R. Cho, R.G.E. Kempen, N.A.J.M. Sommerdijk, J.J. De Yoreo, *Nat. Mater.* **14**, 394 (2015)
62. K. He, M. Sawczyk, C. Liu, Y. Yuan, B. Song, R. Deivanayagam, A. Nie, X. Hu, V.P. Dravid, J. Lu, C. Sukotjo, Y. Lu, P. Král, T. Shokuhfar, R. Shahbazian-Yassar, *Sci. Adv.* **6**, eaaz7524 (2020)
63. X. Liu, S.W. Chee, S. Raj, M. Sawczyk, P. Král, U. Mirsaidov, *Proc. Natl. Acad. Sci. U.S.A.* **118**, e2008880118 (2021)
64. J. Yang, Z. Zeng, J. Kang, S. Betzler, C. Czarnik, X. Zhang, C. Ophus, C. Yu, K. Bustillo, M. Pan, J. Qiu, L.W. Wang, H. Zheng, *Nat. Mater.* **18**, 970 (2019)
65. P. Abellan, T.J. Woehl, L.R. Parent, N.D. Browning, J.E. Evans, I. Arslan, *Chem. Commun.* **50**, 4873 (2014)
66. N.M. Schneider, M.M. Norton, B.J. Mendel, J.M. Grogan, F.M. Ross, H.H. Bau, *J. Phys. Chem. C* **118**, 22373 (2014)
67. T.J. Woehl, P. Abellan, *J. Microsc.* **265**, 135 (2017)
68. D. Zhang, Y. Zhu, L. Liu, X. Ying, C.E. Hsiung, R. Sougrat, K. Li, Y. Han, *Science* **359**, 675 (2018)
69. J.P. Patterson, P. Abellan, M.S. Denny, C. Park, N.D. Browning, S.M. Cohen, J.E. Evans, N.C. Gianneschi, *J. Am. Chem. Soc.* **137**, 7322 (2015)
70. T.J. Woehl, J.E. Evans, I. Arslan, W.D. Ristenpart, N.D. Browning, *ACS Nano* **6**, 8599 (2012)
71. M. Wang, C. Park, T.J. Woehl, *Chem. Mater.* **30**, 7727 (2018)
72. T.H. Moser, H. Mehta, C. Park, R.T. Kelly, T. Shokuhfar, J.E. Evans, *Sci. Adv.* **4**, eaaq1202 (2018)
73. N. Ahmad, G. Wang, J. Nelayah, C. Ricolleau, D. Alloyeau, *Nano Lett.* **17**, 4194 (2017)
74. H.-W. Cheng, S. Yan, J. Li, J. Wang, L. Wang, Z. Skeete, S. Shan, C.J. Zhong, *ACS Appl. Mater. Interfaces* **10**, 40348 (2018)
75. J. Hermannsdörfer, N. de Jonge, A. Verch, *Chem. Commun.* **51**, 16393 (2015)
76. B. Fritsch, T.S. Zech, M.P. Bruns, A. Körner, S. Khadivianazar, M. Wu, N. Zargar Talebi, S. Virtanen, T. Unruh, M.P.M. Jank, E. Spiecker, A. Hutzler, *Adv. Sci.* **9**, 2202803 (2022)
77. B. Fritsch, A. Körner, T. Couasnon, R. Blukis, M. Taherkhani, L.G. Benning, M.P.M. Jank, E. Spiecker, A. Hutzler, *J. Phys. Chem. Lett.* **14**, 4644 (2023)
78. S.W. Chee, U. Anand, G. Bisht, S.F. Tan, U. Mirsaidov, *Nano Lett.* **19**, 2871 (2019)
79. T.J. Woehl, T. Prozorov, *J. Phys. Chem. C* **119**, 21261 (2015)
80. A. Verch, M. Pfaff, N. de Jonge, *Langmuir* **31**, 6956 (2015)
81. S.W. Chee, Z. Baraissov, N.D. Loh, P.T. Matsudaira, U. Mirsaidov, *J. Phys. Chem. C* **120**, 20462 (2016)
82. V. Jamali, C. Hargus, A. Ben-Moshe, A. Aghazadeh, H.D. Ha, K.K. Mandadapu, A.P. Alivisatos, *Proc. Natl. Acad. Sci. U.S.A.* **118**, e2017616118 (2021)
83. S. Kang, J.H. Kim, M. Lee, J.W. Yu, J. Kim, D. Kang, H. Baek, Y. Bae, B.H. Kim, S. Kang, S. Shim, S.J. Park, W.B. Lee, T. Hyeon, J. Sung, J. Park, *Sci. Adv.* **7**, eabi5419 (2021)
84. H. Katsuno, Y. Kimura, T. Yamazaki, I. Takigawa, *Microsc. Microanal.* **28**, 138 (2022)
85. L. Yao, Z. Ou, B. Luo, C. Xu, Q. Chen, *ACS Cent. Sci.* **6**, 1421 (2020)
86. N. de Jonge, L. Houben, R.E. Dunin-Borkowski, F.M. Ross, *Nat. Rev. Mater.* **4**, 61 (2018)
87. S. Jeon, T. Heo, S.Y. Hwang, J. Ciston, K.C. Bustillo, B.W. Reed, J. Ham, S. Kang, S. Kim, J. Lim, K. Lim, J.S. Kim, M.H. Kang, R.S. Bloom, S. Hong, K. Kim, A. Zettl, W.Y. Kim, P. Ercius, J. Park, W.C. Lee, *Science* **371**, 498 (2021)
88. H. Zheng, R.K. Smith, Y. Jun, C. Kisielowski, U. Dahmen, A.P. Alivisatos, *Science* **324**, 1309 (2009)
89. D. Alloyeau, W. Dachraoui, Y. Javed, H. Belkahla, G. Wang, H. Lecoq, S. Ammar, O. Ersen, A. Wisnet, F. Gazeau, C. Ricolleau, *Nano Lett.* **15**, 2574 (2015)
90. H.G. Liao, H. Zheng, *J. Am. Chem. Soc.* **135**, 5038 (2013)
91. T.J. Woehl, C. Park, J.E. Evans, I. Arslan, W.D. Ristenpart, N.D. Browning, *Nano Lett.* **14**, 373 (2014)
92. A. Khelfa, J. Nelayah, H. Amara, G. Wang, C. Ricolleau, D. Alloyeau, *Adv. Mater.* **33**, 2102514 (2021)
93. H.G. Liao, D. Zherebetskyy, H. Xin, C. Czarnik, P. Ercius, H. Elmlund, M. Pan, L.W. Wang, H. Zheng, *Science* **345**, 916 (2014)
94. W. Gao, A.O. Elnabawy, Z.D. Hood, Y. Shi, X. Wang, L.T. Roling, X. Pan, M. Mavrikakis, Y. Xia, M. Chi, *Nat. Commun.* **12**, 3215 (2021)
95. K. Lim, Y. Bae, S. Jeon, K. Kim, B.H. Kim, J. Kim, S. Kang, T. Heo, J. Park, W.C. Lee, *Adv. Mater.* **32**, 2002889 (2020)
96. Y. Bae, K. Lim, S. Kim, D. Kang, B.H. Kim, J. Kim, S. Kang, S. Jeon, J. Cho, W.B. Lee, W.C. Lee, J. Park, *Nano Lett.* **20**, 8704 (2020)
97. X. Zhang, Y. He, M.L. Sushko, J. Liu, L. Luo, J.J. De Yoreo, S.X. Mao, C. Wang, K.M. Rosso, *Science* **356**, 434 (2017)
98. X. Zhang, Z. Shen, J. Liu, S.N. Kerisit, M.E. Bowden, M.L. Sushko, J.J. De Yoreo, K.M. Rosso, *Nat. Commun.* **8**, 835 (2017)
99. C. Zhu, S. Liang, E. Song, Y. Zhou, W. Wang, F. Shan, Y. Shi, C. Hao, K. Yin, T. Zhang, J. Liu, H. Zheng, L. Sun, *Nat. Commun.* **9**, 421 (2018)
100. R.L. Penn, J.F. Banfield, *Science* **281**(5379), 969 (1998)
101. M. Song, G. Zhou, N. Lu, J. Lee, E. Nakouzi, H. Wang, D. Li, *Science* **367**(6473), 40 (2020)
102. B. Jin, M.L. Sushko, Z. Liu, C. Jin, R. Tang, *Nano Lett.* **18**, 6551 (2018)
103. J. Park, H. Elmlund, P. Ercius, J.M. Yuk, D.T. Limmer, Q. Chen, K. Kim, S.H. Han, D.A. Weitz, A. Zettl, A.P. Alivisatos, *Science* **349**, 290 (2015)
104. B.H. Kim, J. Heo, S. Kim, C.F. Reboul, H. Chun, D. Kang, H. Bae, H. Hyun, J. Lim, H. Lee, B. Han, T. Hyeon, A.P. Alivisatos, P. Ercius, H. Elmlund, J. Park, *Science* **368**, 60 (2020)
105. X. Wang, J. Li, H.D. Ha, J.C. Dahl, J.C. Ondry, I. Moreno-Hernandez, T. Head-Gordon, A.P. Alivisatos, *J. Am. Chem. Soc. Au* **1**, 316 (2021)
106. Y. Liu, M. Klement, Y. Wang, Y. Zhong, B. Zhu, J. Chen, M. Engel, X. Ye, *J. Am. Chem. Soc.* **143**, 16163 (2021)
107. Y. Wang, J. Chen, Y. Zhong, S. Jeong, R. Li, X. Ye, *J. Am. Chem. Soc.* **144**, 13538 (2022)
108. S. Merkens, G. De Salvo, J. Kruse, E. Modin, C. Tollan, M. Grzelczak, A. Chuvilin *Ultramicroscopy* **245**, 113654 (2023). https://doi.org/10.1016/j.ultramic.2022.113654
109. Y. Liu, X.M. Lin, Y. Sun, T. Rajh, *J. Am. Chem. Soc.* **135**, 3764 (2013)
110. E. Sutter, P. Sutter, A.V. Tkachenko, R. Krahne, J. de Graaf, M. Arciniegas, L. Manna, *Nat. Commun.* **7**, 11213 (2016)
111. G. Lin, S.W. Chee, S. Raj, P. Král, U. Mirsaidov, *ACS Nano* **10**, 7443 (2016)
112. S.F. Tan, U. Anand, U. Mirsaidov, *ACS Nano* **11**, 1633 (2017)
113. A.S. Powers, H.G. Liao, S.N. Raja, N.D. Bronstein, A.P. Alivisatos, H. Zheng, *Nano Lett.* **17**, 15 (2017)
114. E. Sutter, B. Zhang, S. Sutter, P. Sutter, *Nanoscale* **11**, 34 (2019)
115. E. Cepeda-Perez, D. Doblas, T. Kraus, N. de Jonge, *Sci. Adv.* **6**, eaba1404 (2020)
116. C. Huang, X. Chen, Z. Xue, T. Wang, *Sci. Adv.* **6**, eaba1321 (2020)
117. B. Luo, Z. Wang, T. Curk, G. Watson, C. Liu, A. Kim, Z. Ou, E. Luijten, Q. Chen, *Nat. Nanotechnol.* **18**, 589 (2023)
118. C. Goldmann, W. Chaâbani, C. Hotton, M. Impéror-Clerc, A. Moncomble, D. Constantin, D. Alloyeau, C. Hamon, *Small* **19**, e2303380 (2023)
119. J. Park, H. Zheng, W.C. Lee, P.L. Geissler, E. Rabani, A.P. Alivisatos, *ACS Nano* **6**, 2078 (2012)
120. J. Kim, Z. Ou, M.R. Jones, X. Song, Q. Chen, *Nat. Commun.* **8**, 761 (2017)
121. Y. Zhong, V.R. Allen, J. Chen, Y. Wang, X. Ye, *J. Am. Chem. Soc.* **144**, 14915 (2022)
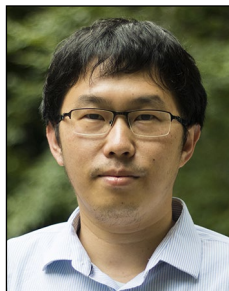
□

Publisher's note
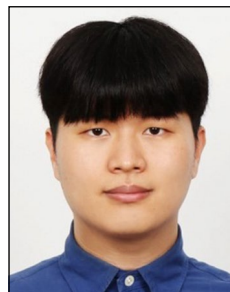
Joodeok Kim is currently a postdoctoral researcher at Seoul National University, South Korea. He received his BS and PhD degrees in chemical and biological engineering from Seoul National University, in 2017 and 2023, respectively. His research primarily focuses on the growth mechanisms of nanoparticles, *in situ* transmission electron microscopy (TEM), and the application of machine learning methods in TEM analysis. Kim can be reached by email at juori22@snu.ac.kr.

Sungsu Kang is currently a postdoctoral researcher at Seoul National University, South Korea. He received his BS degree in 2018 from the School of Chemical and Biological Engineering at Seoul National University, South Korea. He received his PhD degree in 2024 from the School of Chemical and Biological Engineering at Seoul National University. His research interests include *in situ* observation of nanoparticles, aberration-corrected electron microscopy, and liquid phase transmission electron microscopy. Kang can be reached by email at sungsukang@snu.ac.kr.

Fanrui Cheng is a graduate student at Indiana University. He obtained his BS degree in 2021 in chemistry from Southern University of Science and Technology, China. His research interests include liquid phase transmission electron microscopy and nanoparticle self-assembly. Cheng can be reached by email at chengf@iu.edu.

Yi Wang is currently a research engineer at Western Digital. She received her BS degree in 2015 and MPhil degree in 2017 in chemistry from Hong Kong Baptist University, Hong Kong. She received her PhD degree in 2023 from the Department of Chemistry at Indiana University. Her research focuses on the self-assembly of polymer-grafted nanoparticles, colloidal nanoparticle synthesis, ligand engineering, and thin films. Wang can be reached by email at yw90@iu.edu.

Xingchen Ye has been an assistant professor in the Department of Chemistry at Indiana University since 2017. He received his BS degree in chemistry from the University of Science and Technology of China in 2006. He received his PhD degree in chemistry from the University of Pennsylvania in 2012. He then completed postdoctoral work at the University of California, Berkeley, from 2013 to 2016. His research areas include *in situ* electron microscopy of nanomaterials, self-assembly, catalysis, and plasmonics. Ye can be reached by email at xingye@indiana.edu.

Jungwon Park has been an assistant professor in the School of Chemical and Biological Engineering at Seoul National University, South Korea, since 2016. He is also jointly affiliated with the Center for Nanoparticle Research, Institute for Basic Science. He received his BS degree in 2003 from the Department of Chemistry at Pohang University of Science and Technology, South Korea. He received his PhD degree in 2012 from the Department of Chemistry at the University of California, Berkeley. After his PhD, he joined a research group in the School of Engineering and Applied Sciences at Harvard University. His research area includes *in situ* study of nanomaterials, liquid phase transmission electron microscopy, phase transitions, interface chemistry, and low-dimensional materials. Park can be reached by email at jungwonpark@snu.ac.kr.